J|A|C|S
ARTICLES
Published on Web 05/11/2005

New Family of Aminophenalenyl-Based Neutral Radical Molecular Conductors: Synthesis, Structure, and Solid State Properties

Swadhin K. Mandal,[†] Mikhail E. Itkis,[†] Xiaoliu Chi,[†] Satyabrata Samanta,[†] David Lidsky,[‡] Robert W. Reed,[§] Richard T. Oakley,[§] Fook S. Tham,[†] and Robert C. Haddon*[,†]

Contribution from the Departments of Chemistry, Chemical & Environmental Engineering, and Electrical Engineering, University of California, Riverside, California 92521-0403, and Department of Chemistry, University of Waterloo, Waterloo, Ontario N2L3G1, Canada

Received January 14, 2005; E-mail: robert.haddon@ucr.edu

Abstract: We report the preparation, crystallization, and solid-state characterization of the first members of a new family of spiro-bis-(1,9-diamino-substituted-phenalenyl)boron neutral radicals. The crystal structures show that the three radicals are monomeric and without close contacts in the crystal lattice. In all cases magnetic susceptibility measurements confirm the presence of free radicals with one unpaired spin per molecule. Two of the new radical compounds are among the most highly conducting neutral organic solids, with room-temperature conductivities reaching $\sigma_{RT} = 4 \times 10^{-2}$ S/cm. The measured conductivities correlate with the closest intermolecular contacts in the solid state and with the calculated band dispersions, even though the bandwidths are much smaller than those found in other organic conductors.

Introduction

Since the discovery of charge transfer (CT) salts based on 7,7,8,8-tetracyano-*p*-quinodimethane (TCNQ)[1] over 40 years ago, it has been accepted that organic molecular conductors require two components: a donor and an acceptor.[2,3] Recent work has led to the development of single component organometallic neutral molecular conductors with extended tetrathiafulvalene (TTF) dithiolate ligands, such as [Ni(tmdt)$_2$] (tmdt = trimethylenetetrathiafulvalenedithiolate), which exhibits metallic conductivity and three-dimensional Fermi surfaces for both holes and electrons.[4−6] More recently, a single component three-dimensional conductor based on Mo_3S_7 trinuclear clusters with dithiolate ligands has been reported.[7] All these conductors can be classified as single component molecular conductors based on internal charge transfer and the work has been reviewed recently.[8]

Molecular conductors based on single-component neutral-radicals represent an alternative approach to the design of lattices with spins. An array of radicals in a neutral lattice could function like atoms in an elemental metal.[9,10] In this way, the unpaired electrons serve as the charge carriers and orbital overlap between adjacent radicals generates a half-filled energy band. Sulfur−nitrogen radicals were the first class of neutral radicals to show conductivity based on this principle.[11] The idea of using the phenalenyl system as a building block for designing intrinsic molecular conductors and superconductors is not only appealing but also challenging,[9,10] and this system has attracted theoretical and experimental attention.[12−18] Phenalenyl is an odd alternant

[†] Departments of Chemistry and Chemical & Environmental Engineering, University of California, Riverside.
[‡] Department of Electrical Engineering, University of California, Riverside.
[§] University of Waterloo.

(1) Kepler, R. G.; Bierstedt, P. E.; Merrifield, R. E. *Phys. Rev. Lett.* **1960**, *5*, 503−504.
(2) Williams, J. M.; Ferraro, J. R.; Thorn, R. J.; Carlson, K. D.; Geiser, U.; Wang, H. H.; Kini, A. M.; Whangbo, M.-H. *Organic Superconductors (Including Fullerenes)*; Prentice Hall: Englewood Cliffs, NJ, 1992.
(3) Grossel, M. C.; Weston, S. C. *Contemp. Org. Synth.* **1994**, *1*, 367−386.
(4) Tanaka, H.; Okano, Y.; Kobayashi, H.; Suzuki, W.; Kobayashi, A. *Science* **2001**, *291*, 285−287.
(5) Tanaka, H.; Tokumoto, M.; Ishibashi, S.; Graf, D.; Choi, E. S.; Brooks, J. S.; Yasuzuka, S.; Okano, Y.; Kobayashi, H.; Kobayashi, A. *J. Am. Chem. Soc.* **2004**, *126*, 10518−10519.
(6) Kobayashi, A.; Sasa, M.; Suzuki, W.; Fujiwara, E.; Tanaka, H.; Tokumoto, M.; Okano, Y.; Fujiwara, H.; Kobayashi, H. *J. Am. Chem. Soc.* **2004**, *126*, 426−427.
(7) Llusar, R.; Uriel, S.; Vicent, C.; Clemente-Juan, J. M.; Coronado, E.; Gòmez-García, C. J.; Braïda, B.; Canadell, E. *J. Am. Chem. Soc.* **2004**, *126*, 12076−12083.
(8) Kobayashi, A.; Fujiwara, E.; Kobayashi, H. *Chem. Rev.* **2004**, *104*, 5243−5264.
(9) Haddon, R. C. *Nature* **1975**, *256*, 394−396.
(10) Haddon, R. C. *Aust. J. Chem* **1975**, *28*, 2343−2351.
(11) Oakley, R. T. *Can. J. Chem.* **1993**, *71*, 1775−1784.
(12) Goto, K.; Kubo, T.; Yamamoto, K.; Nakasuji, K.; Sato, K.; Shiomi, D.; Takui, T.; Kubota, M.; Kobayashi, T.; Yakusi, K.; Ouyang, J. *J. Am. Chem. Soc.* **1999**, *121*, 1619−1620.
(13) Morita, Y.; Aoki, T.; Fukui, K.; Nakazawa, S.; Tamaki, K.; Suzuki, S.; Fuyuhiro, A.; Yamamoto, K.; Sato, K.; Shiomi, D.; Naito, A.; Takui, T.; Nakasuji, K. *Angew. Chem., Int. Ed. Engl.* **2002**, *41*, 1793−1796.
(14) Fukui, K.; Sato, K.; Shiomi, D.; Takui, T.; Itoh, K.; Gotoh, K.; Kubo, T.; Yamamoto, K.; Nakasuji, K.; Naito, A. *Synth. Met.* **1999**, *103*, 2257−2258.
(15) Koutentis, P. A.; Chen, Y.; Cao, Y.; Best, T. P.; Itkis, M. E.; Beer, L.; Oakley, R. T.; Brock, C. P.; Haddon, R. C. *J. Am. Chem. Soc.* **2001**, *123*, 3864−3871.
(16) Takano, Y.; Taniguchi, T.; Isobe, H.; Kubo, T.; Morita, Y.; Yamamoto, K.; Nakasuji, K.; Takui, T.; Yamaguchi, K. *J. Am. Chem. Soc.* **2002**, *124*, 11122−11130.
(17) Takano, Y.; Taniguchi, T.; Isobe, H.; Kubo, T.; Morita, Y.; Yamamoto, K.; Nakasuji, K.; Takui, T.; Yamaguchi, K. *Chem. Phys. Lett.* **2002**, *358*, 17−23.
(18) Huang, J.; Kertesz, M. *J. Am. Chem. Soc.* **2003**, *125*, 13334−13335.

Scheme 1

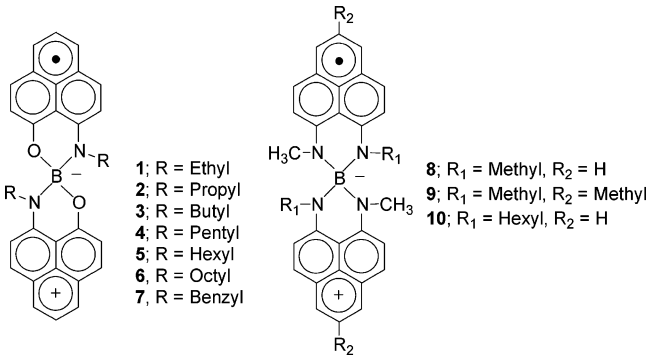

hydrocarbon with high symmetry (D_{3h}) and can exist in three different stable forms: the diamagnetic cation, the paramagnetic radical, the diamagnetic anion, all of which are planar and spectroscopically well characterized.[12−14,19−21] The paramagnetic phenalenyl radicals are prone to dimerization either by π-association or by σ-association. The first report of the solid-state characterization of a dimeric pair of sterically hindered 2,5,8-tri-*tert*-butyl substituted phenalenyl radicals[12] provided a new understanding of the nature of the intermolecular interaction between phenalenyl radicals.[14,16,17,22] Recent work has demonstrated that the intermolecular π-associations in the 2,5,8-tri-*tert*-butyl substituted phenalenyl system can take place by formation of the normal two electron bond to form a π-dimer (radical−radical) that is favored in solution, or by the formation of a one-electron bond to form a π-pimer (radical−cation), which is favored in the solid state.[22]

In our pursuit of phenalenyl-based neutral radical molecular conductors, we have recently reported a series of spiro-bis(1,9-disubstituted phenalenyl)boron neutral radicals, **1**−**7** (Scheme 1).[23−28] Spiro conjugation at the central boron atom leads to an intramolecular $\pi-\pi$ energy level splitting E_1 on the order of 0.5 eV (see Scheme 2), and the lower level is the singly occupied molecular orbital (SOMO) thus generating a quarter-filled energy band in contradistinction to conventional neutral radicals.[18] Since the discovery of the first (monomeric) boron containing neutral radical molecular conductor (**5**) bearing the phenalenyl based N,O-ligand system,[23] we have reported a class of dimeric neutral radical molecular conductors (**1**, **3**) differing only in the length of the alkyl groups (Scheme 1). Radicals **1** and **3** form face to face π-dimers so that there is selective registry between spin-bearing carbon atoms of the phenalenyl units.[24] These dimeric neutral radicals (**1** and **3**) simultaneously exhibit bistability in three physical channels: magnetic, electrical, and optical,[29] which has been rarely realized in a single system.[30] Interestingly, these crystals (**1** and **3**) undergo phase transitions from high-temperature paramagnetic states to low-temperature diamagnetic states, accompanied by an increase in the conductivities by two orders of magnitude. Recently, we reported the first one-dimensional phenalenyl-based neutral radical molecular conductor **7**.[27] In the solid state, phenalenyl units of **7** pack perpendicularly in the *x*- and *z*- directions, whereas the phenalenyl units are parallel to each other in the *y*-direction and pack in a π-step stack fashion. Most recently, we have reported the first example of light mediated C−C σ-bond formation between two radical molecules of **6**.[28] Thus **6** exists as two different forms: a free radical semiconductor and an insulating σ-dimer, and the formation of these crystalline forms is dictated by the presence or absence of light.

Scheme 2

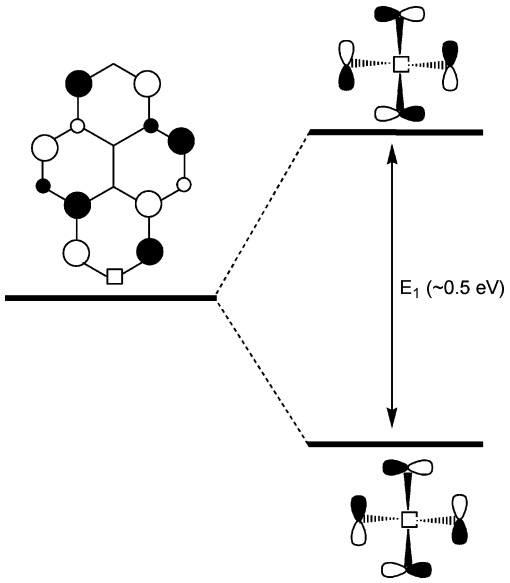

The distinctive features of these molecular solids include: (1) the absence of stacking and obvious conducting pathway(s) in most compounds; (2) versatility in solid-state packing; (3) sensitivity of the structures and solid-state properties to small changes in the pattern of substitution; for example, radical **5** with hexyl substituents[23] on the nitrogen shows the highest conductivity ($\sigma_{RT} = 5 \times 10^{-2}$ S/cm), of any neutral organic solid, while radical **4** with pentyl substituents[26] shows a conductivity of $\sigma_{RT} = 4 \times 10^{-7}$ S/cm which is five orders smaller in magnitude than that of **5**; (4) difficulty in rationalizing the structures, band structures, magnetism, and conductivity to provide a consistent picture of the electronic structure.

There are number of difficulties that must be surmounted if molecular metals and superconductors based on phenalenyl are to be realized, and the current class of compounds directly addresses some of these problems. The presence of perpendicular π-systems effectively inhibits the simple one-dimensional stacking that is characteristic of many organic charge-transfer salts. Radical **7** adopts a 1-D π-step structure, but the packing constraints do not allow efficient overlap, and this compound circumvents the usual charge density wave instabilities that are characteristic of 1-D systems. Due to the fact that there is only

(19) Reid, D. H. *Tetrahedron* **1958**, *3*, 339−352.
(20) Reid, D. H. *Quart. Rev.* **1965**, *19*, 274−302.
(21) Paskovich, D. H.; Reddoch, A. H. *J. Am. Chem. Soc.* **1972**, *94*, 6938−6939.
(22) Small, D.; Zaitsev, V.; Jung, Y.; Rosokha, S. V.; Head-Gordon, M.; Kochi, J. K. *J. Am. Chem. Soc.* **2004**, *126*, 13850−13858.
(23) Chi, X.; Itkis, M. E.; Patrick, B. O.; Barclay, T. M.; Reed, R. W.; Oakley, R. T.; Cordes, A. W.; Haddon, R. C. *J. Am. Chem. Soc.* **1999**, *121*, 10395−10402.
(24) Chi, X.; Itkis, M. E.; Kirschbaum, K.; Pinkerton, A. A.; Oakley, R. T.; Cordes, A. W.; Haddon, R. C. *J. Am. Chem. Soc.* **2001**, *123*, 4041−4048.
(25) Chi, X.; Itkis, M. E.; Reed, R. W.; Oakley, R. T.; Cordes, A. W.; Haddon, R. C. *J. Phys. Chem. B* **2002**, *106*, 8278−8287.
(26) Chi, X.; Itkis, M. E.; Tham, F. S.; Oakley, R. T.; Cordes, A. W.; Haddon, R. C. *Int. J. Quantum Chem.* **2003**, *95*, 853−865.
(27) Pal, S. K.; Itkis, M. E.; Reed, R. W.; Oakley, R. T.; Cordes, A. W.; Tham, F. S.; Siegrist, T.; Haddon, R. C. *J. Am. Chem. Soc.* **2004**, *126*, 1478−1484.
(28) Liao, P.; Itkis, M. E.; Oakley, R. T.; Tham, F. S.; Haddon, R. C. *J. Am. Chem. Soc.* **2004**, *126*, 14297−14302.
(29) Itkis, M. E.; Chi, X.; Cordes, A. W.; Haddon, R. C. *Science* **2002**, *296*, 1443−1445.
(30) Miller, J. S. *Angew. Chem., Int. Ed. Engl.* **2003**, *42*, 27−29.

Scheme 3

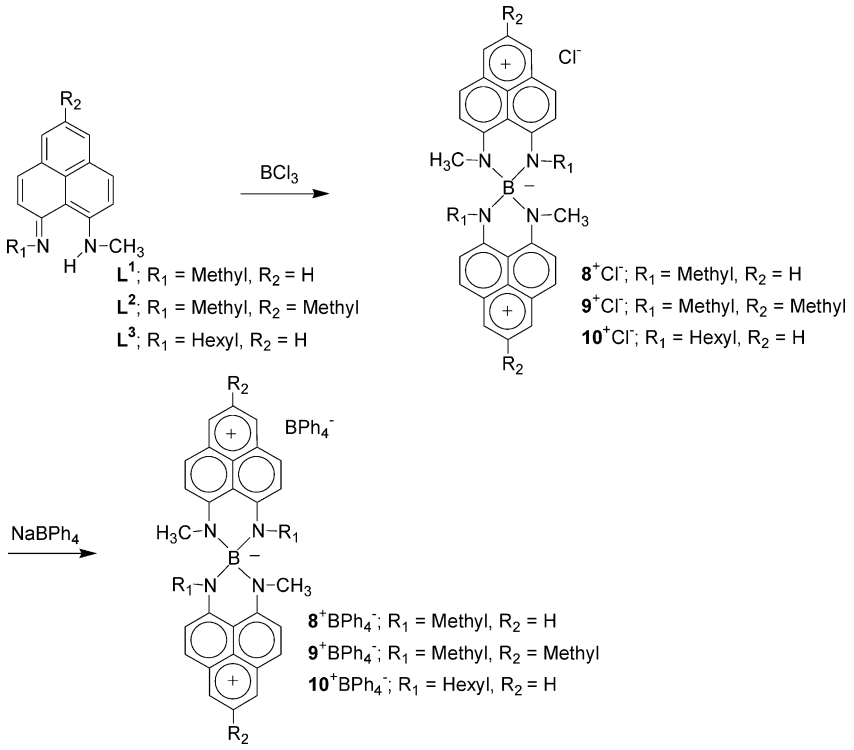

one spin per two phenalenyl rings, the large on-site Coulomb correlation energy (U) which leads to an insulating ground state in most the half-filled band structures[15] is absent in these compounds (although further reduction of U is likely to be important).

We have now crystallized a new family of spiro-bis(1,9-disubstituted-phenalenyl)boron neutral radicals **8**−**10** based on the diaminophenalenyl system (Scheme 1). In the present manuscript, we report the synthesis, electrochemistry, crystallization, and solid-state properties of three radicals (**8**−**10**). In the solid state, these radicals remain monomeric; they do not form σ- or π-dimers. Magnetic susceptibility measurements show that these radicals exist as isolated free radicals with one spin per molecule, although the degree of interaction between the individual molecules in the solid-state dictates the electronic structure, conductivity, and low-temperature magnetic behavior of these three compounds. Two of these radicals are among the most highly conducting neutral organic solids. We assess the strength of the interactions between the molecules in the lattice by using extended Hückel theory (EHT) band electronic structure calculations and discuss some challenges remaining in understanding the relationship between crystal structure, magnetism, optics, and conductivity in this new class of neutral organic solids.

Results and Discussion

Preparation and Electrochemical Properties of Radicals 8−**10.** The syntheses of radicals **8**−**10** followed the same basic procedure that has been used to prepare radicals **1**−**7**.[23,24,27,28] We first prepared the chloride salts (**8**$^+$Cl$^-$−**10**$^+$Cl$^-$), but finally the tetraphenylborate anion is introduced to achieve the required solubility properties (Scheme 3). The tetraphenylborate salts (**8**$^+$-BPh$_4^-$−**10**$^+$BPh$_4^-$) were purified as air-stable, but light sensitive red crystals by recrystallization from methanol and dichloromethane. The electrochemistry of **8**$^+$BPh$_4^-$−**10**$^+$BPh$_4^-$ is presented in Figure 1, where it may be seen that each of these salts shows a well-behaved reversible double reduction corresponding to the successive generation of radical and anion (Scheme 4). The reduction potentials and the disproportionation potentials ($\Delta E^{2-1} = E^2_{1/2} - E^1_{1/2}$) are given in Table 1.

As would be expected based on the electronegativities of the substituents, the reduction potentials of the new compounds

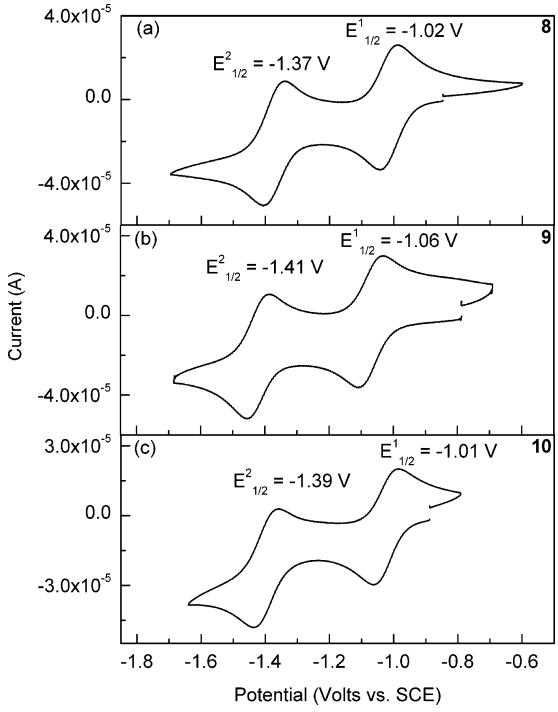

Figure 1. Cyclic voltammetry of (a) **8**$^+$BPh$_4^-$, (b) **9**$^+$BPh$_4^-$, and (c) **10**$^+$BPh$_4^-$ in acetonitrile, referenced to SCE via internal ferrocene (not shown).

Scheme 4

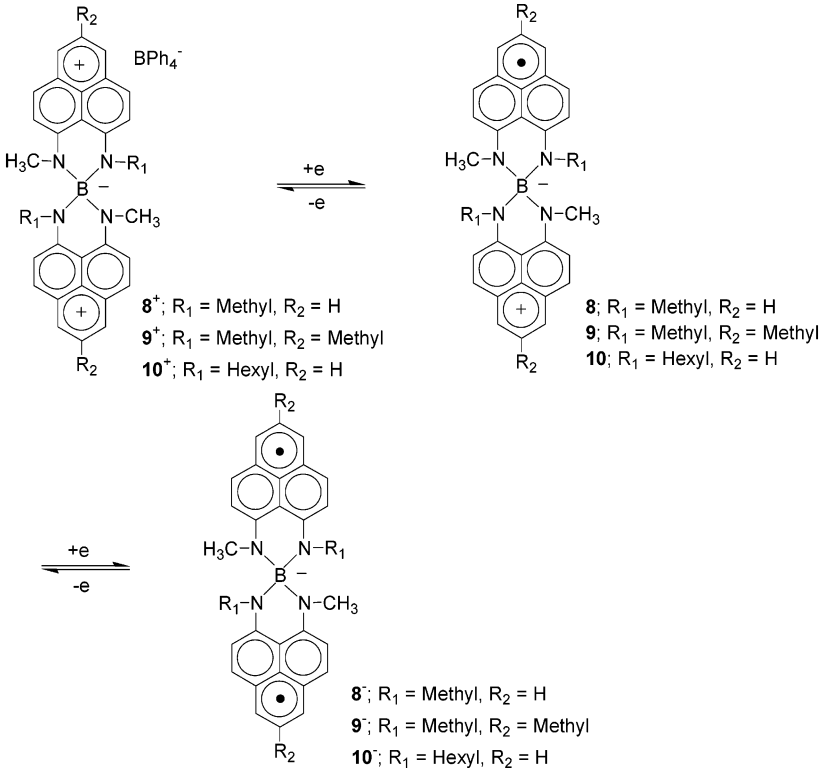

Scheme 5

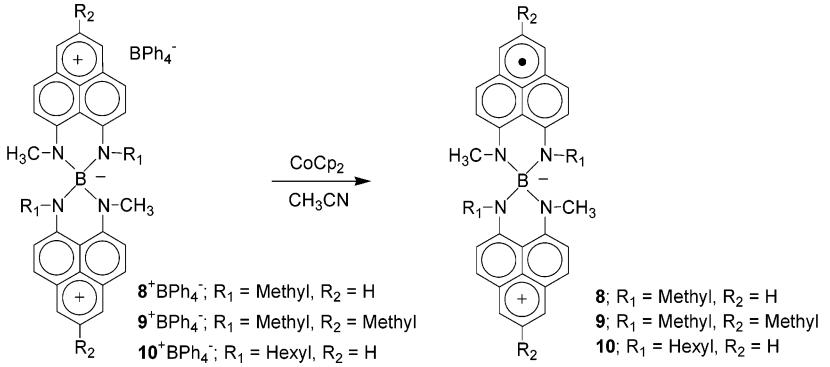

Table 1. The Half-Wave Potentials and Disproportionation Potentials (Volts vs SCE) for Spiro-bis(1,9-disubstituted phenalenyl)boron Salts in CH_3CN

salt	$E^1_{1/2}$	$E^2_{1/2}$	ΔE^{2-1}
1$^+BPh_4^-$	−0.75	−1.10	−0.35
2$^+BPh_4^-$	−0.75	−1.10	−0.35
3$^+BPh_4^-$	−0.73	−1.09	−0.36
5$^+BPh_4^-$	−0.74	−1.11	−0.37
6$^+BPh_4^-$	−0.74	-1.12	−0.38
7$^+BPh_4^-$	−0.68	−1.02	−0.34
8$^+BPh_4^-$	−1.02	−1.37	−0.35
9$^+BPh_4^-$	−1.06	−1.41	−0.35
10$^+BPh_4^-$	−1.01	−1.39	−0.38

(**8**$^+BPh_4^-$−**10**$^+BPh_4^-$), occur at more negative potentials than those of **1**$^+BPh_4^-$−**7**$^+BPh_4^-$, while the disproportionation potentials (ΔE^{2-1}) are very similar. The ΔE^{2-1} value largely determines the on-site Coulomb correlation energy (U) in the solid state, and it is well established as an important discriminator for organic metals.[31,32]

We crystallized the radicals **8**−**10** by use of a chemical reductant (Scheme 5) in an H-cell and obtained moderate yields of high quality, long black needles of radical crystals. Cobaltocene was used as reductant as its oxidation potential ($E^{1/2}$ = −0.91 V)[33] falls slightly below the first reduction potential of **8**$^+BPh_4^-$−**10**$^+BPh_4^-$ salts. To ensure high crystal quality the H-cell was loaded in a drybox and the solvent (acetonitrile) was degassed a minimum of three times on a vacuum line before mixing reductant and salt. Crystal growth started on the glass frit after overnight standing, and the crystals reached their optimum size and quality in about 5−7days. Though solutions of the radical are extremely oxygen sensitive, the crystals are sufficiently stable to allow ambient chemical analyses, X-ray crystal structures, and solid-state measurements.

X-Ray Crystal Structures of 8−10. Table 2 provides crystal data and Figure 2 shows ORTEP drawing of the radicals (**8**−**10**). There are eight molecules of **8** and four molecules of **9**

(31) Garito, A. F.; Heeger, A. J. *Acc. Chem. Res.* **1974**, *7*, 232−240.

(32) Torrance, J. B. *Acc. Chem. Res.* **1979**, *12*, 79−86.

(33) Robbins, J. L.; Edelstein, N.; Spencer, B.; Smart, J. C. *J. Am. Chem. Soc.* **1982**, *104*, 1882−1893.

Table 2. Crystal Data for Radicals **8**−**10**

radical	**8**	**9**	**10**
empirical formula	$C_{30}H_{26}BN_4$	$C_{32}H_{30}BN_4$	$C_{40}H_{46}BN_4$
F_w	453.36	481.41	593.62
temp	218(2) K	223(2) K	223(2) K
color	black	black	black
crystal system	orthorhombic	monoclinic	monoclinic
space group	Pbca	$P2_1/c$	$P2_1/n$
a, Å	19.300(4)	14.293(6)	13.519(3)
b, Å	9.2553(18)	19.354(8)	16.220(4)
c, Å	25.467(5)	9.355(4)	15.878(4)
α, deg	90	90	90
β, deg	90	103.517(14)	112.008(6)
γ, deg	90	90	90
V, Å^3	4549.0(16)	2516.2(18)	3228.1(13)
Z	8	4	4
crystal size, mm	0.55 0.29 0.10	0.32 0.22 0.01	0.55 0.46 0.17
goodness-of-fit, F^2	1.030	1.031	1.061
final *R* indices [$I > 2\sigma(I)$]	R1 = 0.0443, wR2 = 0.0948	R1 = 0.0599, wR2 = 0.1397	R1 = 0.0568, wR2 = 0.1396
R indices (all data)	R1 = 0.0788, wR2 = 0.1209	R1 = 0.1127, wR2 = 0.1619	R1 = 0.0954, wR2 = 0.1721

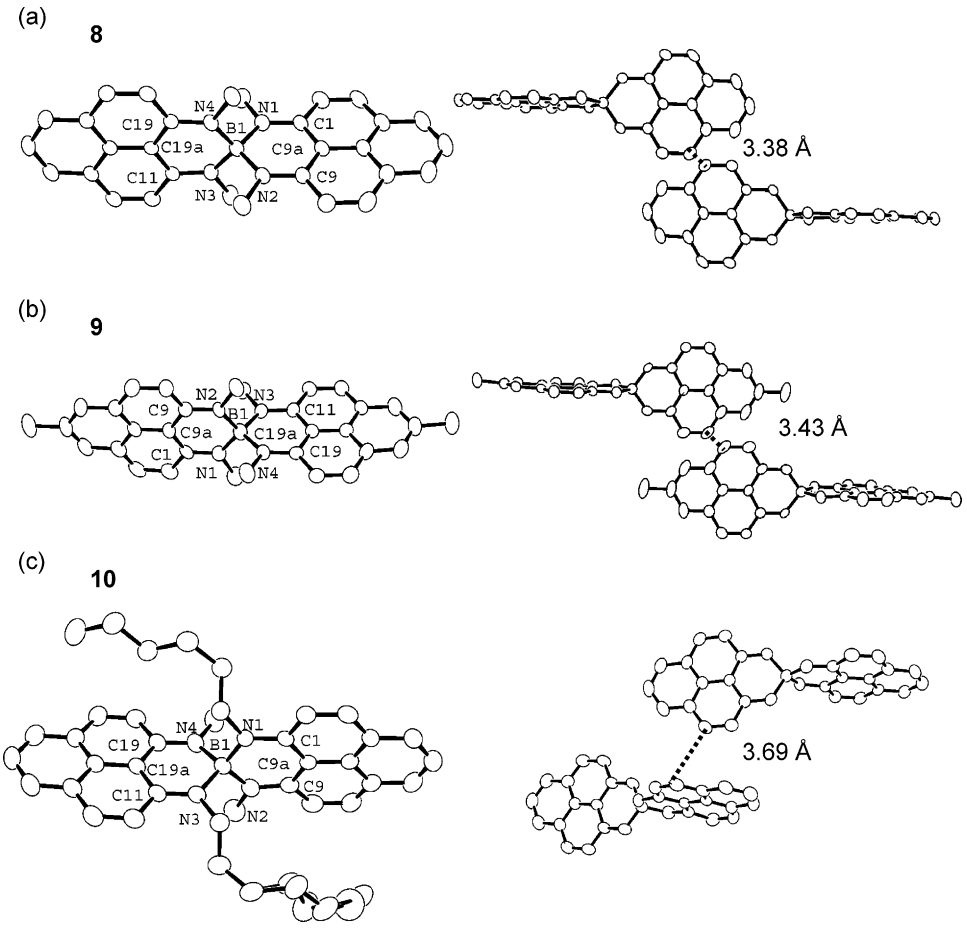

Figure 2. ORTEP diagrams and closest intermolecular C···C distances among the spin bearing carbon atoms of phenalenyl units in the crystal lattice of **8**−**10** (hydrogen atoms are omitted for clarity): (a) radical **8**, (b) radical **9**, and (c) radical **10**. One of the hexyl chains attached to the N(3) atom in radical **10** is disordered (site occupancy ratio of 60% to 40%).

and **10** in their corresponding unit cells. The most important point for our purposes is the absence of simple *σ*- or *π*-dimerization. We did not employ any bulky substituents at the active position of the phenalenyl nucleus in order to suppress intermolecular carbon···carbon bond formation.[15,34,35] Carbon-based free radicals usually require steric hindrance to suppress *σ*-dimerization in the solid state,[12,36] and we are not aware of any other system where resonance stabilization has been sufficient to allow the realization of carbon-based free radicals in the solid state. The radicals **9** and **10** differ from **8** only by the presence of substituents on the phenalenyl ring system (**9**) or the amino substituent (**10**), but each radical adopts an entirely

(34) Haddon, R. C.; Wudl, F.; Kaplan, M. L.; Marshall, J. H.; Cais, R. E.; Bramwell, F. B. *J. Am. Chem. Soc.* **1978**, *100*, 7629−7633.
(35) Haddon, R. C.; Chichester, S. V.; Stein, S. M.; Marshall, J. H.; Mujsce, A. M. *J. Org. Chem.* **1987**, *52*, 711−712.
(36) Griller, D.; Ingold, K. U. *Acc. Chem. Res.* **1976**, *9*, 13−19.

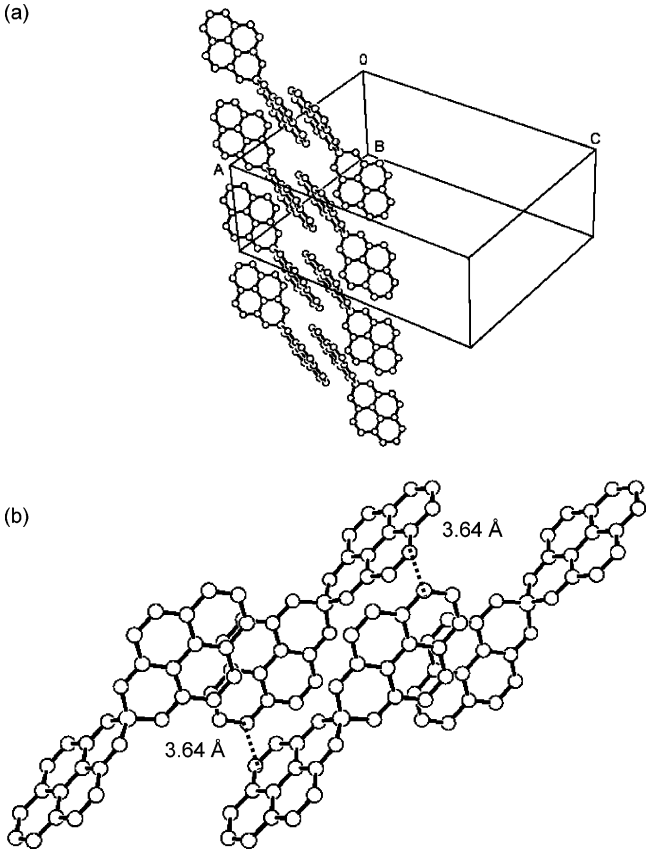

Figure 3. (a) Packing of radical **8** in the *y*-direction showing four pairs of slipped π-dimers (b) Closest intermolecular C···C contacts (3.64 Å) among the spin bearing carbon atoms of phenalenyl units between two pairs of slipped π-dimers in crystalline **8**.

different solid-state structure. The stereoviews down the *x*-axis (see Figure S1 in Supporting Information), indicate a zigzag packing pattern in **8** whereas the other two radicals (**9** and **10**) pack as chains. A closer examination of the packing of molecule **8**, reveals that a pair of spin bearing carbon atoms on adjacent phenalenyl units display an intermolecular distance of 3.38 Å—just below the sum of the van der Waals atomic separations for carbon (3.4 Å for C···C). The closest approach between spin bearing carbon atoms in radical **9** is 3.43 Å, whereas in radical **10** the closest intermolecular distance between spin bearing carbon atoms is 3.69 Å (Figure 2). In terms of intermolecular interactions, it is obvious that radicals **8** and **9** are quite different from radical **10**, and it has been previously established that the orientation of the radicals in the lattice plays the determining role in influencing the conductivity properties.[25] It is clear that the carbon atoms with the shortest intermolecular contacts possess π-orbitals which are oriented for efficient overlap in the case of **8** and **9**, but not **10**.

The most important intermolecular contact in crystalline **8** involves an interaction between a single pair of spin bearing carbon atoms on phenalenyl units of nearest neighbor molecules which are parallel to each other, and we refer to this mode of packing as slipped π-dimers, and this mode of interaction bears an obvious resemblance to the π-step structure of **7**.[27] The slipped π-dimers themselves pack in the direction of the *y*-axis as shown in Figure 3a, and the interaction between pairs of slipped π-dimers is poor as a result of the orientation of the molecules and because the closest approach between carbon

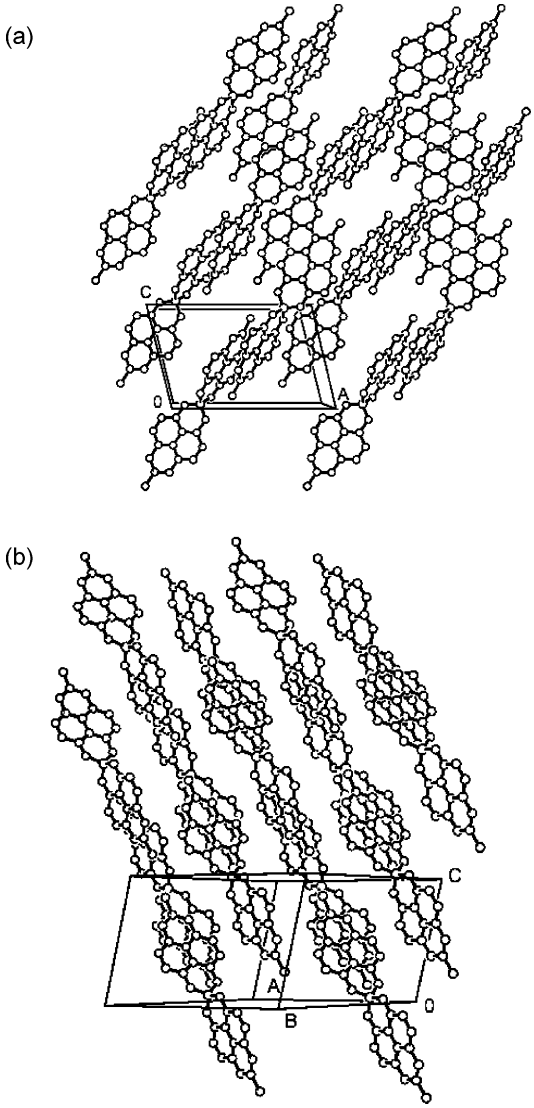

Figure 4. The packing of crystalline **9** showing an infinite array of slipped π-dimers which form chains: (a) viewed down the *y*-axis, (b) a diagonal view.

atoms is 3.64 Å (Figure 3b). The most important feature of the packing of radical **9** is the existence of a continuous array of slipped π-dimers as shown in Figure 4. The closer view shown in Figure 5 makes clear that the two halves of the molecule are not interacting symmetrically with adjacent molecules. The closest intermolecular distance between the two parallel phenalenyl rings ('A' type) is 3.43 Å, whereas for the other two phenalenyl units ('B' type) it is 3.54 Å. The slipped π-dimers that are characteristic of the solid-state packing of radicals **8** and **9** are absent in radical **10**. The phenalenyl units of nearest-neighbor molecules in radical **10** are nearly perpendicular to each other (dihedral angle of 83.4°) with a closest intermolecular distance between the spin bearing carbon atoms of 3.69 Å and the molecules pack in the direction of *y*-axis (Figure 6); the almost perpendicular arrangement of the phenalenyl units in the lattice has been previously shown to lead to very low conductivities.[25] Thus, there are no intermolecular contacts which approach the van der Waals atomic separation in **10**, and it appears that the molecules sit in the lattice completely independent of one another. It seems reasonable to assume that the solid-state packing of these radicals (**8**−**10**) is primarily dictated

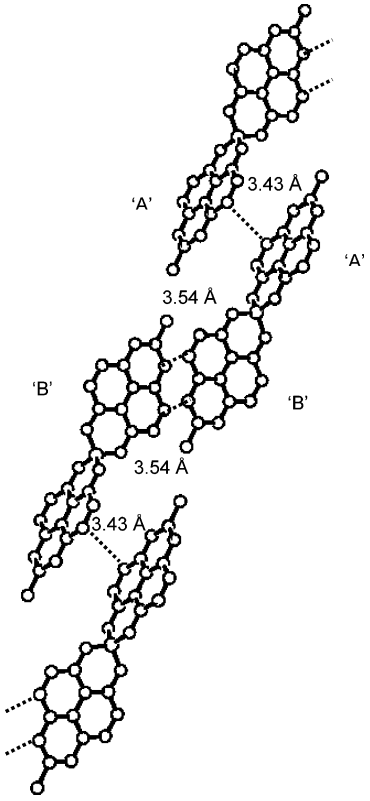

Figure 5. Closest intermolecular C···C contacts (3.54 Å) between two pairs of slipped π-dimers in crystalline **9**.

by steric factors. The hexyl substituents in radical **10** apparently hinder the parallel approach of the neighboring phenalenyl units that is characteristic of the packing of the other two radicals, **8** and **9** which bear smaller substituents (methyl) at the nitrogen atoms.

Magnetic Susceptibility of 8−10. Figure 7a shows the magnetic susceptibilities (χ) of **8**, **9**, and **10** over the temperature range 4−330 K. At high temperatures (T > 100 K for **8**, T > 50 K for **9**, and T > 35 K for **10**), the data can be described by Curie−Weiss behavior $\chi = C/(T-\Theta)$ with Weiss constant $\Theta = -55$, -70, and -14 K and Curie constant $C = 0.36$, 0.37, and 0.34 K*emu/mol for **8**, **9**, and **10,** respectively. The Curie constants are close to 0.375 K*emu/mol, the value expected for a neutral radical with one unpaired spin per molecule. The low-temperature data show significant deviations from Curie−Weiss behavior due to antiferromagnetic coupling of the unpaired spins, with maxima in the $\chi(T)$ curves at $T_{MAX} = 42$, 33, and 20 K for **8**, **9**, and **10**, respectively.

We used the analytical representation[37] of the Bonner−Fisher model for the $S = 1/2$ antiferromagnetic Heisenberg chain of isotropically interacting spins[38] to fit χ(T) for compound **10** in temperature range 10−330 K (Figure 7a), and we obtained an intrachain exchange constant $J = -10.1$ cm^{-1}. We were unable to obtain a satisfactory fit to the magnetic date of compounds **8** and **9** with this model, but we found that the alternating antiferromagnetic Heisenberg chain model[39] in which the antiferromagnetic interaction along the chain alternates between values of J and αJ ($0 \leq \alpha \leq 1$), provided satisfactory

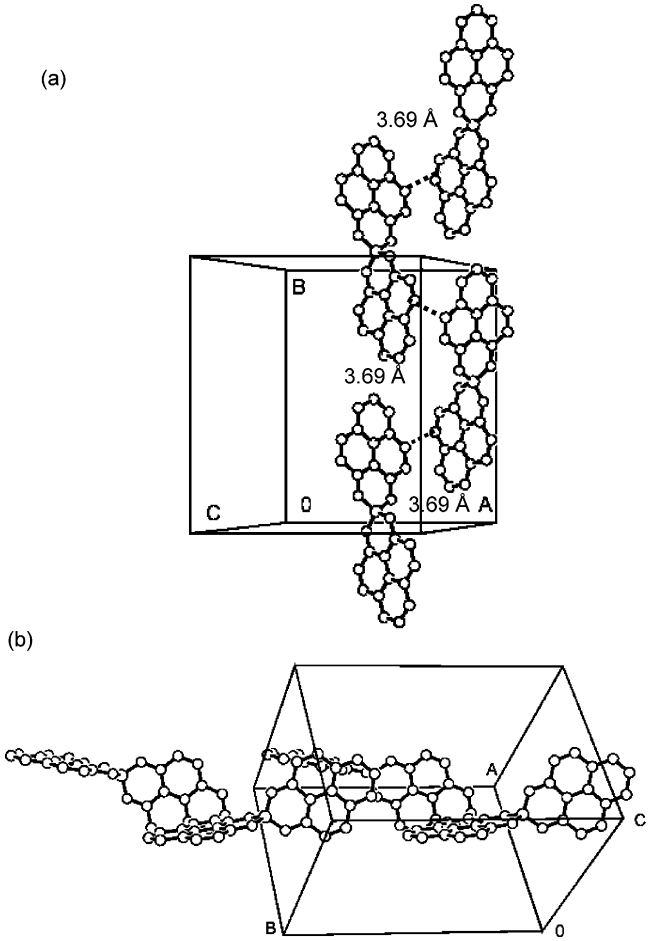

Figure 6. Packing of crystalline **10**: (a) showing the closest intermolecular distance between the spin bearing carbon atoms of the phenalenyl units which repeat along the y-direction, and (b) a different view showing the adjacent phenalenyl units that are approximately perpendicular to each other.

fits for compound **8** in the temperature range 20−330 K ($J = -26.6$ cm^{-1}, $\alpha = 0.8$), and for compound **9** in the temperature range 16−150 K ($J = -19.7$ cm^{-1}, $\alpha = 0.6$). The utilization of the alternating antiferromagnetic Heisenberg chain model is appropriate in the case of compounds **8** and **9** because the crystallographic structures show alternating intermolecular separation between spin-bearing atoms along the chain directions: 3.38 and 3.64 Å (compound **8**, Figure 3) and 3.43 and 3.54 Å (compound **9**, Figure 5), while for compound **10** there is no alternation (Figure 6a). The antiferromagnetic coupling along the 1-D chains dominates the temperature dependence of the magnetic susceptibility at low temperatures although contributions from alternative magnetic pathways involving interchain coupling cannot be completely excluded (Figure S2 of Supporting Information); the strong antiferromagnetic interactions suppress the Curie spin count per molecule (χ*T/0.375) at low temperatures (Figure 7b).

Electrical Conductivity of 8−10. The single-crystal electrical conductivities (σ) of **8**−**10** were measured using four-probe contacts, and the temperature dependence of the conductivity is shown in Figure 8. A number of crystals were evaluated with similar results. The values of the room-temperature conductivities are $\sigma_{RT} = 4 \times 10^{-2}$ S/cm (**8**) and 1×10^{-2} S/cm (**9**); these values are among the highest obtained for neutral organic solids and are comparable to radicals **1** (1.0×10^{-2} S/cm), **3** (2.4×10^{-2} S/cm), and **5** (4.9×10^{-2} S/cm).[23,24] The room-temperature

(37) Estes, W. E.; Gavel, D. P.; Hatfield, W. E.; Hodgson, D. J. *Inorg. Chem.* **1978**, *17*, 1415−1421.
(38) Bonner, J. C.; Fisher, M. E. *Phys. Rev.* **1964**, *135*, A640.
(39) Duffy, W.; Barr, K. P. *Phys. Rev.* **1968**, *165*, 647−654.

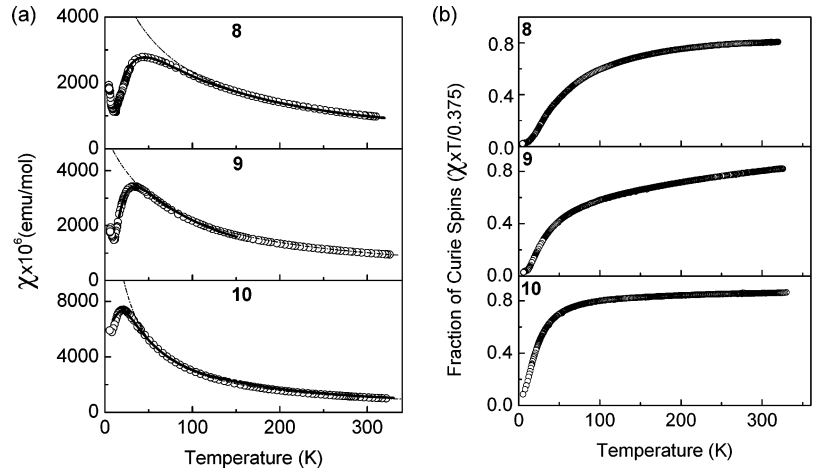

Figure 7. (a) Magnetic susceptibility of crystalline **8**−**10** as a function of temperature; the dashed lines represent the Curie−Weiss fit, whereas the solid lines represent the fits by the alternating-Heisenberg-linear-chain model for **8** and **9**, and uniform-Heisenberg-chain model for **10**. (b) Fraction of Curie spins of crystalline **8**−**10** as a function of temperature.

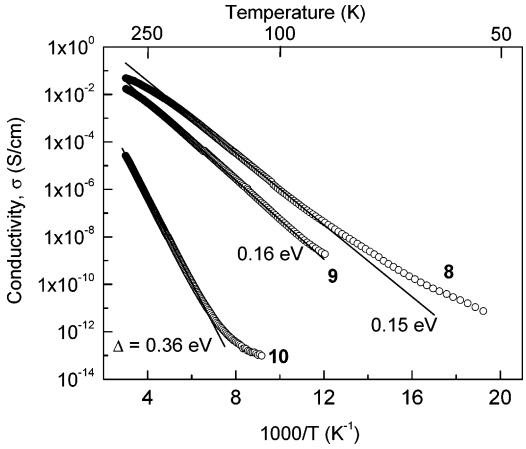

Figure 8. Single-crystal conductivity of **8**−**10** as a function of temperature.

conductivity of **10** is 4 orders of magnitude smaller ($\sigma_{RT} = 7 \times 10^{-6}$ S/cm) and is comparable with radical **2** (1.4×10^{-6} S/cm) and radical **4** (4×10^{-7} S/cm).[25,26] The conductivity data show semiconducting temperature dependence with activation energies of $\Delta = 0.15$ (**8**), 0.16 (**9**), and 0.36 eV (**10**).

Optical Measurements of 8−**10.** To obtain further information on the electronic structure, we measured the transmission spectra of single crystals of **8**−**10** and the results are presented in Figure 9a; transmission measurements are possible because of the needlelike morphology of the crystals, some of which are quite thin. The most important feature in the transmission spectra is the strong increase of absorption that occurs between 0.40 ($E_{g'}$) and 0.47 eV (E_g) for radical **8**, 0.41 ($E_{g'}$) and 0.49 eV (E_g) for radical **9**, and 0.46 ($E_{g'}$) and 0.57 eV (E_g) for radical **10**, (where E_g is the frequency of the absorption onset and $E_{g'}$ is the frequency where the absorption reaches a plateau), and it is apparent that the fundamental absorption edges are quite broad in these radicals. The measured optical band gap (E_g or $E_{g'}$) can sometimes be correlated with the activation energy (Δ) calculated from the temperature dependence of the conductivity ($E_g \approx 2 \times \Delta$). The absorptions in the mid-IR from 650 to 3000 cm^{-1} are due to the molecular vibrations of the radicals.

We performed solution phase IR measurements of the radicals in dichloromethane in order to better understand the nature of the solid state near-IR (NIR) absorptions (Figure 9b). The absorption at ~0.5 eV in the NIR solution spectra results from excitations from the singly occupied molecular orbital (SOMO) to the lowest unoccupied molecular orbital (LUMO); these orbitals (SOMO and LUMO) result from the spiro-interaction between the symmetrical and antisymmetrical combinations of

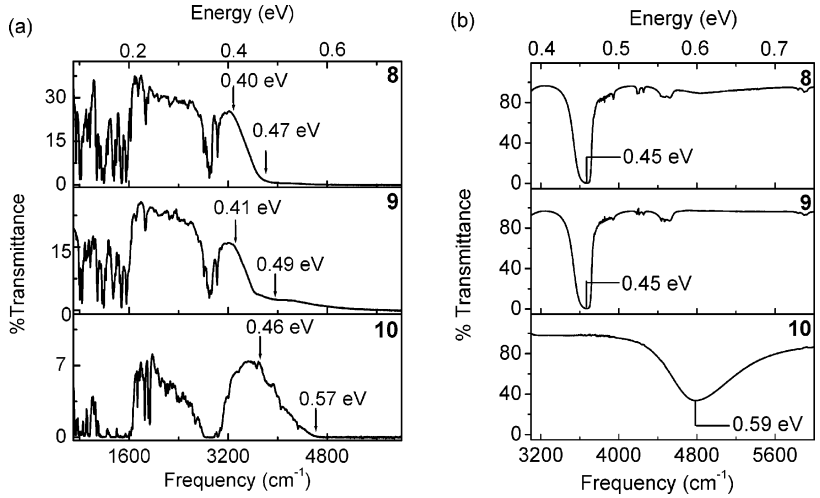

Figure 9. IR and UV−visible transmission spectra of: (a) single crystals of **8**−**10** and (b) solution of **8**−**10** in dichloromethane.

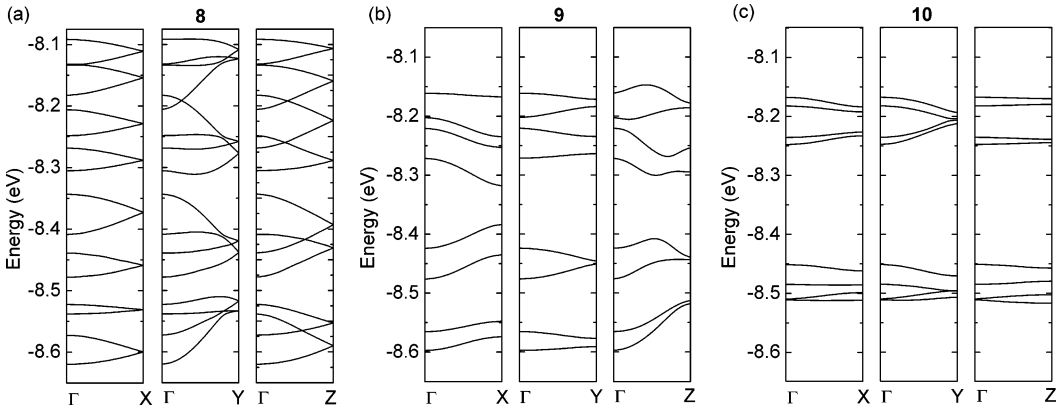

Figure 10. Calculated band structures of: (a) crystalline **8**, (b) crystalline **9**, and (c) crystalline **10**.

the 1,9-disubstituted-phenalenyl molecular orbitals (Scheme 2).[40] The solution spectra show absorption maxima at lower energy (0.45 eV) for **8** and **9**, than is observed for radical **10** (0.59 eV), indicating that the gap between SOMO and LUMO in **8** and **9** is smaller than that in **10**.

Band Electronic Structure of 8, 9, and 10. To address the question of solid-state packing and the electronic structure of **8**−**10**, we carried out extended Hückel theory (EHT) band structure calculations[41] on the crystal structures. Such calculations have been very useful in understanding the electronic structure of the organic molecular superconductors[42] and thin-film field effect transistors,[43] but it should be noted at the outset that there are certain objections to the application of tight binding band theory to the neutral radical molecular conductors,[23] in that the calculations are unable to correctly describe the open shell electronic structure of the materials as indicated by the occurrence of Curie paramagnetism. A characteristic feature of the previously reported radicals (**1**−**5**) has been the very narrow bandwidths found with the EHT calculations. The band dispersion found for these compounds is usually less than 0.1 eV, whereas most organic metals show EHT bandwidths in the range 0.5−1.0 eV.[2,42,43] Radical **7** proved to be an exception with a 1-D π-step structure resulting in Heisenberg antiferromagnetism, a substantial band dispersion (0.37 eV, along b*), indicative of metallic character and no observable superlattice.[27] However, radical **7** exhibits semiconducting behavior with a low room-temperature conductivity of $\sigma_{RT} = 1.4 \times 10^{-3}$ S/cm which is very difficult to reconcile with the structure and remaining properties.

Figure 10 shows the results of the band structure calculations carried out on the lattices found in the X-ray crystal structures. The bands (sixteen bands for **8** and eight bands for each of **9** and **10**) are derived from the SOMO and the LUMO of **8**, **9** and **10** of the molecules in the unit cell (eight molecules for **8** and four molecules for **9** and **10**); these basically consist of the symmetric and antisymmetric combinations of the 1,9-disubstituted phenalenyl cation LUMO.[23,40] Alternatively, they can be viewed as arising from the nonbonding molecular orbitals[9,10] of each of the phenalenyl units in the unit cell (sixteen phenalenyl units for **8** and eight phenalenyl units for each of **9** and **10**). In a tight-binding band picture, these orbitals (sixteen for **8** and eight for each of **9** and **10**) now accommodate a total of eight electrons for **8** and four electrons for each of **9** and **10**, leading to a quarter-filled band complex. The tight binding picture fails, of course, because the magnetic susceptibility shows that the electrons are unpaired at most temperatures.

Table 3. Measured and Calculated Solid-State Parameters for Radicals **8**−**10**

radical	shortest distance (Å)	max. band dispersion (eV)	σ_{RT} (S/cm)	Δ (eV)	E_g (E_g') (eV)	J (cm^{-1})
8	3.38	0.085	4×10^{-2}	0.15	0.47 (0.40)	−26.6
9	3.43	0.078	1×10^{-2}	0.16	0.49 (0.41)	−19.7
10	3.69	0.034	7×10^{-6}	0.36	0.57 (0.46)	−10.1

It may be seen that the band dispersions found for **8** and **9** are higher than **10**. The maximum dispersions are 0.035 (along a*), 0.085 (b*), and 0.05 eV (c*) in **8**, 0.045 eV (along a*), 0.024 eV (b*), and 0.078 eV (c*) in **9**, and 0.016 (along a*), 0.034 (b*), and 0.006 eV (c*) in **10**. The band dispersions reflect the trends observed in the conductivity data: **8** has the highest conductivity and the highest band dispersion, whereas **10** has the lowest conductivity and band dispersion in the series.

Relationship between Solid-State Structure, Conductivity, Magnetism, Optical Spectra, and Band Structure in 8, 9, and 10. We have proposed that the spiro-bis(1,9-disubstituted phenalenyl)boron neutral radical (**5**) can be described as a degenerate Mott−Hubbard insulator with a localized ground state,[23] and this model provides a reasonable picture of the electronic structure of the spiro-bis(1,9-disubstituted phenalenyl)boron neutral radicals isolated to date. Typically, the conductivity in molecular conductors depends on the relationship between the bandwidth (W) and the on-site Coulomb correlation energy (U), which often determines the activation energy for the conductivity (Δ), so that $\Delta \approx U$. Since U is primarily a molecular property that is often related to the disproportionation potential ΔE,[2−1] it is to be expected that the values of U should be similar for radicals **8**, **9**, and **10**, whereas we observe $\Delta =$ 0.15, 0.16, and 0.36 eV for **8**, **9**, and **10** respectively. Thus the bare value of U provides a lower bound for Δ, which is subject to reduction by the solid-state packing and finite bandwidths observed for the radicals (**8**−**10**). The room-temperature conductivities of **8** and **9** are similar while the measured room-temperature conductivity for radical **10** is smaller by 4 orders of magnitude. Table 3 lists various important measured and calculated solid-state parameters. These parameters clearly correlate with the observed intermolecular separation for **8**, **9**,

(40) Haddon, R. C.; Chichester, S. V.; Marshall, J. H. *Tetrahedron* **1986**, *42*, 6293−6300.
(41) Hofmann, R. *Solids and Surfaces*; VCH: New York, 1988.
(42) Haddon, R. C.; Ramirez, A. P.; Glarum, S. H. *Adv. Materials* **1994**, *6*, 316−322.
(43) Haddon, R. C.; Siegrist, T.; Fleming, R. M.; Bridenbaugh, P. M.; Laudise, R. A. *J. Mater. Chem* **1995**, *5*, 1719−1724.

and **10**. The band dispersions correlate with the strength of the antiferromagnetic interactions as manifested by the increase in the magnitude of the *J*-values: −10.1, −19.7, and −26.6 cm^{-1}, for compounds **10**, **9**, **8**, respectively (Table 3 and Figure 7a). The conductivity data show semiconducting temperature-dependent activation energies: $\Delta = 0.15$ (**8**), 0.16 (**9**), and 0.36 eV (**10**), thus demonstrating a trend of increasing Δ with increasing intermolecular separation. The closest intermolecular distance between the spin bearing carbon centers is 3.38 Å in radical **8**, and this compound shows the highest conductivity in the series, whereas radical **10** shows the lowest conductivity and the largest intermolecular separation (3.69 Å).

The precise mechanism of conduction in this class of compounds remains to be explained, but it is apparent that the low on-site Coulomb correlation energy plays an important role and allows effective carrier transport despite the relatively large intermolecular separations. The interactions between neighboring molecules are dominated by their orientation, and in the case of **8** and **9** the neighboring molecules are better oriented for intermolecular π-orbital overlap than **10**, where the adjacent phenalenyl units are nearly perpendicular to each other—an arrangement that has previously been shown to lead to very low conductivities (as in the case of **2**).[25] The spiro conjugation at the central boron atom dictates the energy level splitting between the phenalenyl units (E_1) and this gap is larger (0.59 eV) for radical **10** than for **8** and **9** (~0.45 eV), as observed in the solution IR spectra. Additional splitting of the levels due to intermolecular interaction in the solid state can lead to a reduction of the optical gap[18] and hence the optical band gap (E_g or $E_{g'}$) will depend also on the solid-state bandwidths of the radicals. The electrochemical data (Figure 1, Table 1) suggest similar values for the on-site Coulomb correlation energies (U) of compounds **8**, **9**, and **10**, while the activation energy of the conductivity (Δ) is significantly larger in the case of **10**, than for **8** and **9** (Table 3), which correlates with the optical gaps (E_g, Table 3). This suggests that only those charge carriers that are thermally excited to antibonding states across the observed optical gap E_g ($E_{g'}$) (Table 3) participate in the conductivity. It is therefore apparent that conductivity can be limited by the bandwidths (W) or the on-site Coulomb correlation energy (U), as expected for compounds close to the degenerate Mott limit.

Conclusion

By changing the donor atoms and the substituents, a new family of spiro-bis(1,9-disubstituted phenalenyl)boron neutral radical conductors based on N,N-ligand system has been synthesized and characterized and the solid-state properties investigated. The disproportionation energies, which largely determine the on-site Coulomb correlation energy in the solid state, are very similar to the spiro-bis(1,9-disubstituted phenalenyl)boron neutral radicals based on N,O-ligand system reported previously (**1**−**7**). This is reflected in the measured conductivity of this new class of materials which resembles closely that observed for spiro-bis(1,9-disubstituted phenalenyl)-boron neutral radical based on N,O-ligand system. Two of the radicals (**8** and **9**) are among the most highly conducting neutral organic solids. The conductivity of the solid is largely determined by the molecular packing; nevertheless these radicals show weak intermolecular interactions and the conducting pathways are very subtle in comparison with the classical organic conductors (TTF and C_{60} charge-transfer salts). In this particular case, the measured room-temperature conductivities show an inverse relationship with the closest intermolecular distance in the solid state and a direct relationship with the maximum band dispersions obtained from EHT calculations.

Experimental Section

Materials. All reactions and manipulations were carried out under an atmosphere of dry argon using standard Schlenk and vacuum-line techniques. Triethyloxonium tetrafluoroborate (Fluka), hexylamine (Aldrich), 1.0 M boron trichloride solution in CH_2Cl_2 (Aldrich), sodium tetraphenylborate (Aldrich), and cobaltocene (Strem) were used as received. 9-Hydroxy-1-oxophenalene, 9-hydroxy-5-methyl-1-oxophenalene,[44] and 9-*N*-methylamino-1-oxophenalene[45] were synthesized according to literature procedures. Toluene was distilled from sodium benzophenone ketyl immediately before use. Acetonitrile was distilled from P_2O_5 and then redistilled from CaH_2 immediately before use. The NMR spectra were recorded on a Varian Inova 300 spectrometer. Chemical shifts downfield from the reference standard were assigned positive values. Cyclic voltammetric measurements were performed on a Pine AFCBP1 potentiostat using a Pt wire electrode in dry acetonitrile under argon atmosphere with n-Bu_4NPF_6 as the supporting electrolyte with a saturated calomel reference electrode. The ferrocenium/ferrocene couple was used as internal reference.

9-*N*-Methylamino-5-methyl-1-oxophenalene. A mixture of 9-hydroxy-5-methyl-1-oxophenalene (2.1 g, 10 mmol) and aqueous methylamine (15 mL, 70% solution) was placed in a heavy-walled sealed tube with an Ace thread at one end and sealed with Teflon plug (Ace Glass Inc., Vineland, NJ). The contents were stirred at 125 °C for 7 h. The mixture was allowed to cool, the tube was vented, opened, and the contents were poured into 100 mL of distilled water. The aqueous mixture was extracted with benzene, and the organic layer was separated, dried with sodium sulfate. The solvent was removed with a rotary evaporator, and the crude product was purified by column chromatography on Al_2O_3 with chloroform to give an analytically pure orange solid of the title compound (1.72 g, 77%). mp 117 °C. ^{1}H NMR ($CDCl_3$): δ11.95 (b, 1H), 7.94 (d, 1H), 7.78 (d, 1H), 7.69 (s, 2H), 7.17 (d, 1H), 6.98 (d, 1H), 3.22 (d, 3H), 2.55 (s, 3H). IR (600−4000 cm^{-1}): 3028(w), 2920(w), 1637(m), 1606(w), 1597(m), 1570(m), 1533(s), 1506(w), 1483(w), 1435(w), 1418(w), 1383(w), 1358(w), 1299(m), 1280(m), 1247(m), 1222 (w), 1176(m), 1157(s), 1109(w), 1070(w), 1061(w), 963 (w), 920(m), 876(m), 836(s), 811(m), 784(w), 750(m), 702(w), 675(m). Anal. Calcd for $C_{15}H_{13}NO$: C, 80.67; H, 5.88; N, 6.27. Found: C, 80.51; H, 5.83; N, 6.28.

9-*N*-Methylamino-1-*N*′-methylimino-phenalene (L^1). Triethyloxonium tetrafluoroborate (1.140 g, 6 mmol) was added to a solution of 9-*N*-methylamino-1-oxophenalene (1.255 g, 6 mmol) in 40 mL dry CH_2Cl_2. The solution immediately turned wine-red, and then a yellow precipitate formed. The reaction mixture was stirred 10 h at 25 °C, and then methylamine (6 mL 2M solution in MeOH, 12 mmol) was added, whereupon the yellow precipitate dissolved to give a deep red solution. The reaction mixture was stirred at 25 °C for an additional 6 h. The mixture was poured into 50 mL distilled water; the organic layer was separated and dried over sodium sulfate. The solvent was removed with a rotary evaporator and the crude product was purified by column chromatography on Al_2O_3 with ethyl ether to give an analytically pure red crystalline solid ($\mathbf{L^1}$) (1.0 g, 75%). mp 173 °C (lit mp 147 °C).[46] ^{1}H NMR ($CDCl_3$): δ13.05 (b, 1H), 7.70−7.76 (m, 4H), 7.23−7.35 (m, 3H), 3.39 (s, 6H). IR (600−4000 cm^{-1}): 3041(w), 2971(w), 2859(w), 1635(s), 1608(s), 1587(s), 1522(s), 1470(w), 1399(m), 1366(m), 1301(m), 1247(w), 1230(w), 1186(m), 1157(s), 1118(m), 1065(w), 965(w), 921(m), 909(w), 832(s), 815(vs), 778(m), 755(m), 730(w), 680-

(44) Haddon, R. C.; Rayford, R.; Hirani, A. M. *J. Org. Chem.* **1981**, *46*, 4587−4588.
(45) Haddon, R. C.; Chichester, S. V.; Mayo, S. L. *Synthesis* **1985**, 639−641.
(46) Franz, K. D.; Martin, R. L. *Tetrahedron* **1978**, *34*, 2147−2151.

(s). Anal. Calcd for $C_{15}H_{14}N_2$: C, 81.03; H, 6.36; N, 12.60. Found: C, 81.42; H, 6.44; N, 12.51.

9-*N*-Methylamino-5-methyl-1-*N*′-methylimino-phenalene (L^2). Triethyloxonium tetrafluoroborate (1.44 g, 7.6 mmol) was added to a solution of 9-*N*-methylamino-5-methyl-1-oxophenalene (1.70 g, 7.6 mmol) in 50 mL dry CH_2Cl_2. The solution immediately turned wine-red, and then a yellow precipitate formed. The reaction mixture was stirred 2 h at 25 °C, and then methylamine (8 mL 2M solution in MeOH, 16 mmol), was added whereupon the yellow precipitate dissolved to give a deep red solution. The reaction mixture was stirred at 25 °C for an additional 6 h. The mixture was poured into 100 mL distilled water; the organic layer was separated and dried over sodium sulfate. The solvent was removed with a rotary evaporator to yield a dark red pasty solid, and this was purified by column chromatography on Al_2O_3 with ethyl ether to give an analytically pure red solid ($\mathbf{L^2}$) (1.1 g, 61%). mp 109 °C. ^{1}H NMR ($CDCl_3$): δ12.83 (b, 1H), 7.63 (d, 2H), 7.54 (s, 2H), 7.19 (d, 2H), 3.35 (s, 6H), 2.52 (s, 3H). IR (600−4000 cm^{-1}): 2963-(w), 2924(w), 2859(w), 1631(m), 1604(vs), 1579(m), 1527(s), 1466-(m), 1399(s), 1362(m), 1312(m), 1276(m), 1170(s), 1120(w), 1074(w), 1039(w), 963(m), 930(s), 865(s), 844(w), 813(s), 784(m), 759(w), 744 (w). Anal. Calcd for $C_{16}H_{16}N_2$: C, 81.32; H, 6.82; N, 11.85. Found: C, 81.11; H, 6.87; N, 11.77.

9-*N*-Methylamino-1-*N*′-hexylimino-phenalene (L^3). Triethyloxonium tetrafluoroborate (0.57 g, 3 mmol) was added to a solution of 9-*N*-methylamino-1-oxophenalene (0.63 g, 3 mmol) in 20 mL dry CH_2Cl_2. The solution immediately turned wine-red, and then a yellow precipitate formed. The reaction mixture was stirred 10 h at 25 °C, and then hexylamine (0.80 mL, 6 mmol) was added, whereupon the yellow precipitate dissolved to give a deep red solution. The reaction mixture was stirred at 25 °C for additional 6 h. The mixture was poured into 50 mL water; the organic layer was separated and dried over sodium sulfate. The solvent was removed with a rotary evaporator, and the crude product was purified by column chromatography on Al_2O_3 with ethyl ether to give an analytically pure orange solid ($\mathbf{L^3}$) (0.725 g, 83%). mp 61 °C. ^{1}H NMR ($CDCl_3$): δ13.33 (b, 1H), 7.63−7.72 (m, 4H), 7.28 (t, 1H), 7.21 (d, 1H), 7.20 (d, 1H), 3.60 (m, 2H), 3.35 (s, 3H), 1.84 (m, 2H), 1.56 (m, 2H), 1.40 (m, 4H), 0.94 (t, 3H). IR (600−4000 cm^{-1}): 2959(w), 2937(w), 2863(m), 1652(w), 1633(s), 1608(s), 1587(m), 1573(m), 1520(s), 1470(m), 1366(s), 1310(m), 1245-(w), 1228(w), 1182(s), 1163(s), 961(w), 919(s), 834(s), 819(s), 757-(m), 738(m), 679(s). Anal. Calcd for $C_{20}H_{24}N_2$: C, 82.13; H, 8.28; N, 9.58. Found: C, 82.41; H, 8.46; N, 9.44.

Preparation of $\mathbf{8^+Cl^-}$. 9-*N*-Methylamino-1-*N*′-methylimino-phenalene ($\mathbf{L^1}$, 0.31 g, 1.4 mmol) in chlorobenzene (60 mL) was treated with boron trichloride (0.7 mL 1 M solution in CH_2Cl_2, 0.7 mmol) under argon in the dark, and the mixture was refluxed for 20 h. The red precipitate was isolated by filtration (0.26 g, 76%). MS (MALDI), m/z = 453. IR (600−4000 cm^{-1}): 3083(w), 2989(w), 2881(w), 1633-(s), 1577(s), 1520(s), 1495(m), 1458(m), 1424(w), 1418(w), 1403(w), 1364(w), 1349(s), 1322(m), 1310(m), 1252(m), 1205(m), 1162(s), 990-(s), 903(m), 884(w), 853(m), 842(s), 822(m), 784(m), 740(m), 690-(m).

Preparation of $\mathbf{9^+Cl^-}$. 9-*N*-Methylamino-5-methyl-1-*N*′-methylimino-phenalene ($\mathbf{L^2}$, 0.49 g, 2.1 mmol) in chlorobenzene (50 mL) was treated with boron trichloride (1.0 mL 1 M solution in CH_2Cl_2, 1 mmol) under argon in the dark, and the mixture was refluxed for 18 h. The red precipitate was isolated by filtration (0.48 g, 93%). MS (MALDI), m/z = 481. IR (600−4000 cm^{-1}): 3003(w), 2920(w), 1631(m), 1591(s), 1524(s), 1481(m), 1458(w), 1420(m), 1366(s), 1347(m), 1318(m), 1289-(m), 1197(m), 1166(m), 992(s), 969(w), 876(s), 823(m), 788(w), 698-(m), 684(w).

Preparation of $\mathbf{10^+Cl^-}$. 9-*N*-Methylamino-1-*N*′-hexylimino-phenalene ($\mathbf{L^3}$, 0.61 g, 2.1 mmol) in toluene (30 mL) was treated with boron trichloride (1.0 mL 1 M solution in CH_2Cl_2, 1 mmol) under argon in the dark, and the mixture was refluxed for 14 h. The red sticky oil was separated by decantation of toluene; residual solvent was evaporated under reduced pressure and used for the next step without further purification. MS (MALDI), m/z = 593.

Preparation of $\mathbf{8^+BPh_4^-}$. A solution of 0.30 g of $NaBPh_4$ (0.87 mmol) in 10 mL MeOH was added to a solution of $\mathbf{8^+Cl^-}$, (0.25 g, 0.51 mmol) in 10 mL of MeOH. A red precipitate formed immediately. The mixture was stirred for 15 min, and the red solid was separated by filtration and stored in the dark. The crude product can be purified by recrystallization from dichloromethane/methanol mixture to give red crystals of the title compound (0.3 g, 76%). MS (MALDI), m/z = 453. ^{1}H NMR (CD_3CN): δ 8.35 (d, 4H), 8.19 (d, 4H), 7.68 (t, 2H), 7.46 (d, 4H), 7.27 (m, 8H), 6.98 (t, 8H), 6.83 (t, 4H), 3.05 (b, 12H). IR (600−4000 cm^{-1}): 3058(w), 3006(w), 1627(s), 1577(s), 1539(w), 1516(s), 1493(w), 1474(w), 1456(w), 1424(m), 1417(m), 1362(m), 1349(s), 1320(s), 1251(m), 1203(m), 1161(m), 986(s), 901(m), 882(w), 840-(m), 822(w), 815(w), 763(w), 748(w), 734(s), 705(s). Anal. Calcd for $C_{54}H_{46}B_2N_4$: C, 83.95; H, 6.00; N, 7.25. Found: C, 83.71; H, 5.95; N, 6.90.

Preparation of $\mathbf{9^+BPh_4^-}$. A solution of 0.5 g of $NaBPh_4$ (1.46 mmol) in 10 mL MeOH was added to a solution of $\mathbf{9^+Cl^-}$, (0.5 g, 0.97 mmol) in 10 mL of MeOH. A red precipitate formed immediately. The mixture was stirred for 15 min, and the red solid was separated by filtration and stored in the dark. The crude product can be purified by recrystallization from dichloromethane/methanol mixture to give red crystals of the title compound (0.57 g, 73%). MS (MALDI), m/z = 481. ^{1}H NMR (CD_3CN): δ 8.29 (d, 4H), 8.02 (s, 4H), 7.43(d, 4H), 7.26 (m, 8H), 6.99 (t, 8H), 6.84 (t, 4H), 3.02 (b, 12H), 2.61 (s, 6H). IR (600−4000 cm^{-1}): 3010(w), 2971(w), 2928(w), 2869(w), 1633(s), 1593(s), 1522(s), 1483(s), 1424(s), 1372(s), 1343(m), 1326(m), 1316-(s), 1291(s), 1197(m), 1162(s), 992(s), 969(w), 901(w), 874(m), 826-(s), 748(m), 734(s), 709(s). Anal. Calcd for $C_{56}H_{50}B_2N_4$: C, 83.99; H, 6.30; N, 6.99. Found: C, 84.01; H, 6.38; N, 7.11.

Preparation of $\mathbf{10^+BPh_4^-}$. A solution of 0.72 g of $NaBPh_4$ (2.1 mmol) in 10 mL MeOH was added to a solution of $\mathbf{10^+Cl^-}$, (0.78 g, 1.24 mmol) in 30 mL of MeOH. An orange precipitate formed immediately. The mixture was stirred for 15 min, and the orange solid was separated by filtration and stored in the dark. The crude product can be purified by recrystallization from dichloromethane/methanol mixture to give red microcrystals of the title compound 0.19 g (17%). ^{1}H NMR (CD_3CN): 8.36 (d, 2H), 8.32 (d, 2H), 8.18 (d, 4H), 7.67 (t, 2H), 7.47 (d, 2H), 7.38 (d, 2H), 7.27 (m, 8H), 6.98 (t, 8H), 6.83 (t, 4H), 3.38 (m, 4H), 3.08 (b, 6H), 1.64 (m, 2H), 1.48 (m, 2H), 1.12 (m, 4H), 0.95 (m, 8H), 0.52 (t, 6H). IR (600−4000 cm^{-1}): 3058(w), 2959 (w), 2928(m), 2869(w), 1632(s), 1588(s), 1515(s), 1493(m), 1453(m), 1408(w), 1358(m), 1347(w), 1328(m), 1255(m), 1207(m), 1161(m), 1036(w), 988(m), 961(m), 905(s), 842(s), 821(m), 736(m), 703(s). Anal. Calcd for $C_{64}H_{66}B_2N_4$: C, 84.19; H, 7.30; N, 6.14. Found: C, 83.85; H, 7.27; N, 6.23.

Crystallization of 8. An invertible H-cell with a glass D frit was loaded in a drybox. A solution of 50 mg of $\mathbf{8^+BPh_4^-}$ (0.065 mmol) in 12 mL dry acetonitrile was placed in one container, and 15 mg of $CoCp_2$ (0.080 mmol) dissolved in 12 mL of dry acetonitrile in the other container. The H-cell was removed from the drybox and attached to the vacuum line, and the containers were taken through three cycles of freeze, pump, and thaw to degas the solutions. The H-cell was inverted slowly, and the solutions were allowed to diffuse through the glass frit. After sitting in the dark for one week, the cell yielded 17 mg of black shining crystals. IR (600−4000 cm^{-1}): 3036(w), 2889(w), 1629-(m), 1577(m), 1547(m), 1522(w), 1481(m), 1470(m), 1445(w), 1402-(s), 1362(w), 1351(w), 1324(w), 1257(s), 1205(m), 1170(m), 1130(m), 1114(m), 1078(w), 920(s), 828(m), 805(m), 742(m), 709(w), 688(w), 671(w). Anal. Calcd for $C_{30}H_{26}BN_4$: C, 79.48; H, 5.78; N, 12.36. Found: C, 79.10; H, 6.02; N, 12.33.

Crystallization of 9. An invertible H-cell with a glass D frit was loaded in a drybox. A solution of 112 mg of $\mathbf{9^+BPh_4^-}$ (0.14 mmol) in 15 mL dry acetonitrile was placed in one container, and 32 mg of $CoCp_2$ (0.17 mmol) was dissolved in 16 mL of dry acetonitrile in the other

container. The H-cell was removed from the drybox and attached to the vacuum line, and the containers were taken through three cycles of freeze, pump, and thaw to degas the solutions. The H-cell was inverted slowly and the solutions were allowed to diffuse through the glass frit. After sitting in the dark for one week the cell yielded 24 mg of black shining crystals. IR (600−4000 cm^{-1}): 2907(w), 2812(w), 1635(m), 1595(m), 1558(s), 1531(s), 1476(s), 1458(w), 1453(w), 1414(s), 1366-(m), 1347(m), 1310(s), 1285(w), 1253(w), 1212(s), 1187(s), 1159(s), 1122(s), 1097(s), 990(m), 963(w), 907(vs), 807 (s), 790 (w), 688 (s). Anal. Calcd for $C_{32}H_{30}BN_4$: C, 79.82; H, 6.29; N, 11.63. Found: C, 79.12; H, 6.11; N, 11.59.

Crystallization of 10. An invertible H-cell with a glass D frit was loaded in a drybox. A solution of 91 mg of $\mathbf{10}^{+}BPh_4^{-}$ (0.1 mmol) in 10 mL dry acetonitrile was placed in one container, and 23 mg of $CoCp_2$ (0.12 mmol) was dissolved in 11 mL of dry acetonitrile in the other container. The H-cell was removed from the drybox and attached to the vacuum line, and the containers were taken through three cycles of freeze, pump, and thaw to degas the solutions. The H-cell was inverted slowly and the solutions were allowed to diffuse through the glass frit. After sitting in the dark for one week the cell yielded 14 mg of black shining crystals. IR (600−4000 cm^{-1}): 2954(w), 2932(w), 2859(w), 1631(s), 1585(s), 1558(w), 1520(s), 1497(w), 1456(s), 1416(w), 1349-(m), 1326(w), 1274(w), 1251(w), 1232(w), 1203(w), 1157(m), 1036-(w), 986(w), 963(m), 940(w), 899(m), 840(s), 819(s), 759(m), 694 (m). Anal. Calcd for $C_{40}H_{46}BN_4$: C, 80.91; H, 7.82; N, 9.43. Found: C, 80.38; H, 7.72; N, 9.65.

X-ray Crystallography. Data were collected on a Bruker SMART 1000 platform-CCD X-ray diffractometer system (Mo-radiation, $\lambda = 0.71073$ Å). The crystals were coated with paratone oil and mounted on glass fiber. The crystallographic parameters and unit cell dimensions are summarized in Table 2. Absorption corrections were applied to the raw intensity data using the SADABS program in the SAINTPLUS software package.[47] The Bruker SHELXTL (Version 6.10) software package[48] was used for phase determination and structure refinement. Atomic coordinates, isotropic, and anisotropic displacement parameters of all the non-hydrogen atoms were refined by means of a full matrix least-squares procedure on F^2. All H-atoms were included in the refinement in calculated positions riding on the atoms to which they were attached. Full details, including bond lengths and bond angles, are given in the Supporting Information.

Magnetic Susceptibility Measurements. The magnetic susceptibility was measured with a George Associates Faraday balance operating at 0.5 T.

Conductivity Measurements. The single-crystal conductivities, σ, of **8**, **9**, and **10** were measured in a four-probe configuration. The in-line contacts were made with silver paint. The sample was placed on a sapphire substrate, and electrical connections between the silver paint contacts and substrate were made by thin, flexible 25 μm diameter silver wires to relieve mechanical stress during thermal cycling of the sample. The temperature dependence of the conductivity was measured along long axis of the crystals in the range 332−52 K for **8**, 332−83 K for **9**, and 312−109 K for **10**. The data are presented for the crystals with dimensions 2.00 × 0.25 × 0.03 mm^3 for **8**, 1.60 × 0.16 × 0.03 mm^3 for **9**, and 1.4 × 0.59 × 0.16 mm^3 for **10**. The measurements were carried out in a custom-made helium variable-temperature probe using a Lake Shore 340 temperature controller. A Keithley 236 unit was used as a voltage source and current meter, and two 6517 Keithley electrometers were used to measure the voltage drop between the potential leads in a four-probe configuration.

Single-Crystal Optical Spectroscopy. The infrared transmission measurements were carried out on a FTIR Nicolet Nexus 670 ESP spectrometer integrated with a Continuum Thermo-Nicolet FTIR microscope.

Band Structure Calculations. The band-structure calculations were performed by using a modified version of the extended Hückel theory (EHT) band-structure program supplied by M.-H. Whangbo. The parameter set is chosen to provide a reasonably consistent picture of bonding in heterocyclic organic compounds.[43,49]

Acknowledgment. This work was supported by the Office of Basic Energy Sciences, Department of Energy under Grant No. DE-FG02-04ER46138.

Supporting Information Available: Additional structural packing diagrams, tables of crystallographic and structural refinement data, atomic coordinates, bond lengths, bond angles, and anisotropic thermal parameters (PDF). This information is available free of charge via the Internet at http://pubs.acs.org. See any current masthead page for ordering information and Web access instructions.

JA0502728

(47) 5.02 ed.; Bruker Analytical X-Ray System, Inc: Madison, WI, 1997−1998.
(48) 6.10 ed.; Bruker Analytical X-Ray System, Inc.: Madison, WI, 2000.
(49) Cordes, A. W.; Haddon, R. C.; Oakley, R. T.; Schneemeyer, L. F.; Waszczak, J. V.; Young, K. M.; Zimmerman, N. M. *J. Am. Chem. Soc.* **1991**, *113*, 582−588.